Design and Analysis of a Quasi-TM_{03} Mode *G*-Band Extended Interaction Radiation Source

Yifan Zu,[1] Xuesong Yuan,[1,a)] Xiaotao Xu,[1] Qingyun Chen,[1] Matthew Cole,[2] Yong Yin,[1] Liangjie Bi,[1] Hailong Li,[1] Bin Wang,[1] Lin Meng,[1] and Yang Yan[1]

AFFILIATIONS

[1]Terahertz Science and Technology Key Laboratory of Sichuan Province, School of Electronic Science and Engineering, University of Electronic Science and Technology of China, Chengdu 610054, China

[2]Department of Electronic and Electrical Engineering, University of Bath, North Road, Bath BA2 7AY, UK

[a)]Author to whom correspondence should be addressed: yuanxs@uestc.edu.cn

A disk-loaded coupled cavity structure operating in the quasi-TM_{03} mode has been here used to develop a high electron efficiency, high output power terahertz radiation source, demonstrated that it is possible to concentrate the axial field energy along the source's central axis within a large cavity. Compared with traditional extended interaction devices operating at the same frequency band, the operating mode of this present device provides a sizeable beam tunnel capacity that can support efficient energy conversion between the electron beam and the high frequency field. The developed electron optical system is based on a cylindrical electron beam of 0.3 mm radius, and is capable of producing a beam current of 0.65 A at a bias of 16.4 kV. Particle in cell (PIC) simulations show that such new design approaches can achieve kilowatt-level output power at 0.22 THz, with a high electron efficiency of 11.5%.

I. INTRODUCTION

Advances in microfabrication technology and new security threats considerations have stimulated intense interest in the development of ever more powerful, coherent sources of millimeter-wave (MMW) to terahertz (THz) electromagnetic radiation sources with emission ranging from 0.1 to 10 THz [1], [2]. Due to its wide bandwidth, high directionality, and commensurate high spatial and temporal resolution, a wide variety of new applications have come to the fore, including deep space research, advanced communications, novel radar, remote high-resolution imaging, as well as border protection, threat detection, biological spectroscopy and biomedical diagnostics [3]–[8].

Typically, electronic sources of coherent electromagnetic radiation are based on converting the kinetic energy of a flow of electrons into electromagnetic field energy [4]. In the sub-millimeter and THz regions, solid-state devices are fundamentally restricted due to the inability to pass high currents in an interacting region due to the generation of excessive heat and damaging dielectric breakdown [2]. Vacuum-based devices do not experience such physical limitations. Vacuum electronic devices (VEDs) as a result provide new technological horizons and opportunities in the generation of high power and high efficiency electromagnetic radiation [9]–[12]. VEDs can be divided into two main categories: longitudinal and transverse current modulation devices [4]. Since longitudinal-current-modulation devices do not require a strong magnetic field, their design is dramatically simplified and their application range is, as a result, wider and includes traveling wave tubes (TWTs), extended-interaction klystrons (EIKs), and backward wave oscillators (BWOs) [13]–[18]. Although VEDs have good prospects as MMW-to-THz sources, a number of challenges remain to be solved, chief amongst which are the efficiency and stability of the beam-wave interaction caused by the high frequency (HF) system.

When operating frequencies move to the THz regime, simple scaling commonly used at lower frequencies is not applicable [4]. The dimensions of THz VEDs are usually small, commonly in the millimeter or micron range, since the operating wavelength must be compatible with the dimensions of the HF system. Though the size of the HF system can indeed be scaled, other factors such as the beam-wave interaction stage and the need for suitably sized thermal dissipation stages are becoming increasingly challenging to engineer due to increases in the energy density with VEDs. As frequency increases, the diameter of the beam tunnel shrinks rapidly. In the G-band, the beam tunnel radius of a double corrugated waveguide slow-wave structure (SWS) TWT is $\leq$ 0.1mm [19], [20]. Such small beam tunnels would cause excessive thermal damage as a result of channel interception and which would, as a result, make is increasingly difficult for the electron optical system to provide the necessary high current density. There is a pressing need to develop a large-scale beam tunnel that can support efficient energy conversion between the electron beam and the HF field.

The collective contraction of the design would pose new challenges associated with increasing the output power and electron efficiency. In a typical W-Band EIK, only about 70% of the electromagnetic energy can be coupled to the output waveguide, the remaining 30% being dissipated in the circuit as ohmic losses [21]. For a G-band extended interaction oscillator (EIO), the utilization rate of electrons is less than 2% [22]. As operating frequencies continue to increase further toward the THz regime, more energy is lost in the form of heat. This severely restricts the output power and electronic efficiency of the circuit. One solution is the use of high-order mode operation. In contrast to the fundamental mode commonly used, high-order modes can support a physically larger HF system for a given frequency, so as to enlarge the power capacity. To date, higher-order mode operation has been explored and applied to the ladder-type cavity [23]. However, such devices have low HF field energy in the axial direction of the interaction region. In addition, operating in such higher-order mode circuits generally lowers the resonators characteristic impedance, which makes it possible to be suppressed by fundamental modes.

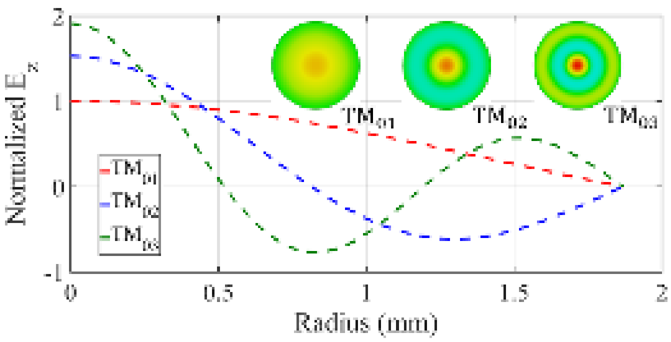

Fig. 1. Normalized electric field amplitude as a function of cavity radius and mode. Insets: the E_z - field contours at cross section of TM_{01}, TM_{02}, and TM_{03} modes.

In response to these challenges, here, we report on a THz extended interaction device for a disk-loaded coupled cavity operating in quasi-TM_{03} mode. Compared with the traditional interaction circuit, such systems support an axial electric field that is strongest on and near the central axis of the cavity, which is very conducive to the interaction with the electron beam passing through the central axis. Moreover, since the Bessel-function field distribution in the radial direction of the cross-section, the higher the order of the TM mode, the more concentrated the electric field in the beam tunnel, and the greater the characteristic impedance, which is extremely beneficial to suppress the generation of fundamental modes. Fig. 1 shows the field amplitude distribution of the TM mode on the cavity radius after normalization based on the maximum amplitude of the TM_{01} mode in the circular waveguide resonator. The dimension of the beam tunnel has been significantly increased due to the more concentrated field energy distribution, thereby alleviating the demanding requirements on the electron optical system. Finally, the axial output not only has a higher output level than the lateral output, but also reduces the challenges caused by processing and assembly. The specific design for making a stably operated circuit with the quasi-TM_{03} mode is realized and demonstrated below. Through parametrically optimized particle in cell (PIC) simulation, such new design approaches have demonstrated superior HF field and beam interaction and in doing open up new technological prospects for the promotion of plasma physics related to the field of generating powerful radiation output from MMW to THz regime.

II. Design and Simulation

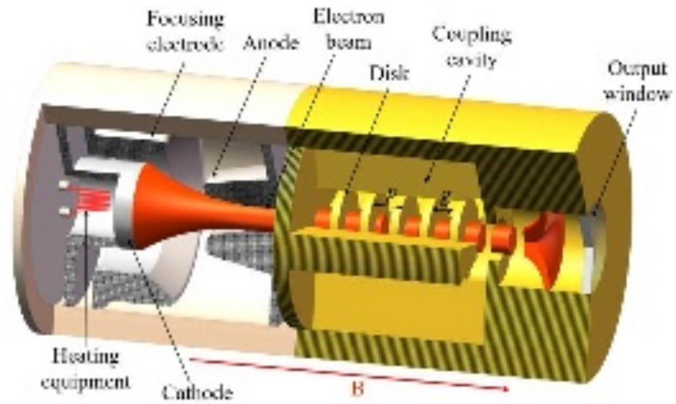

Fig. 2. Schematic depiction of the proposed terahertz oscillator circuit.

TABLE I
DESIGN PARAMETERS

Symbol	Description	Value and Unit
N	Number of gaps	12
p	Length of period	0.32 mm
g	Width of gap	0.14 mm
d_{out}	Outer diameter of disk	0.94 mm
d_{in}	Inner diameter of disk	0.60 mm
o	Output window diameter	1.90 mm
l	Coupling cavity radius	1.73mm
t	Angular width of coupling cavity	70°
V	Voltage	16.40 kV
I	Current	0.65 A
B	Magnetic field strength	0.85 T

Fig. 2 shows a schematic of the THz extended interaction radiation source for the disk-loaded coupled cavity. The device is mainly composed of a thermionic electron optical system, a SWS with disk-loaded coupled cavity structure, an output waveguide, and insulators. The present SWS is a periodic standing-wave circuit composed of 12 interaction gaps in the longitudinal direction. As shown in Fig. 2, electrons are thermally emitted a heated filament. The emitted electrons are then compressed under the combined action of the electric field and the magnetic field to form an electron beam which is accelerated by the anode bias into the beam tunnel. The compressed electron beam enters the beam-wave interaction resonant SWS. Here the quasi-TM_{03} mode is initiated and interacts with the electronic beam. The maximum axial field energy of the quasi-TM_{03} mode is coupled to the output waveguide, and electromagnetic radiation is finally generated in the form of TM_{01} mode. The design parameters are given in Table I. In view of the current microfabrication technology, each part of the device can be made of the oxygen-free copper and manufactured through nano-computer numerical control

(Nano-CNC) machining technology [24] or ultraviolet photolithography and electroforming technique (UV-LIGA) [25].

A. *Mode Analysis*

Extended interaction devices support a range of eigenmodes. Established beam-wave interaction theory shows that the electron beam interacts with the E_z component of the electric field, making it crucial in selecting the TM mode [26], [27]. To illustrate the advantages of the disk-loaded coupled cavity circuit in terms of beam-mode coupling and beam-wave interaction, the CST eigenmode solver has been used to analyze the HF characteristics. Based on the same operating frequency, the operating circuits of the typical ladder-type structure in the fundamental mode and the higher-order mode have been considered. Fig. 3 shows the electric field distribution of the three circuits.

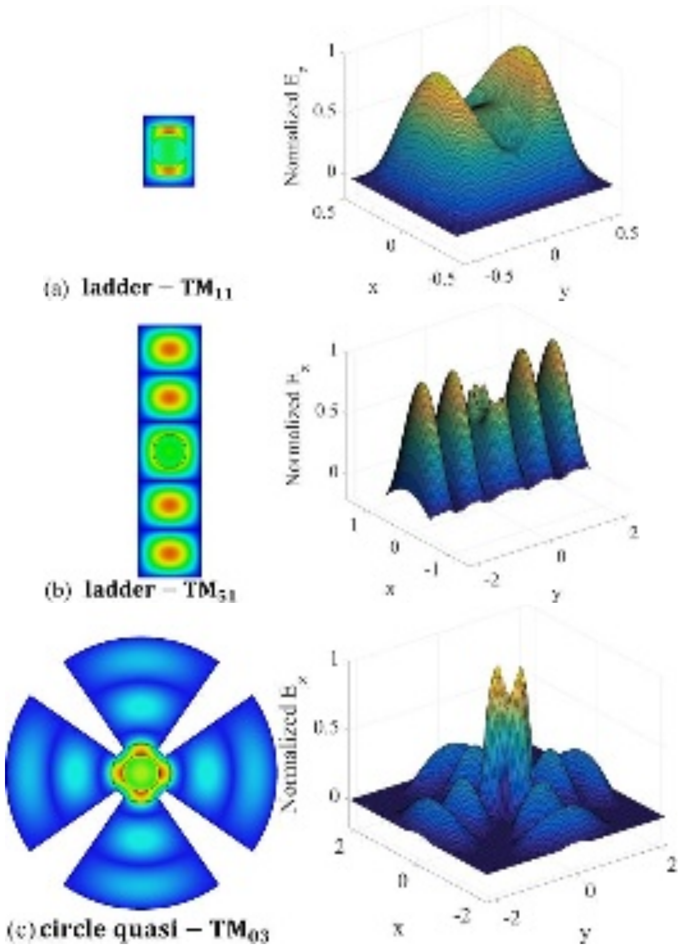

Fig. 3. Cross –sectional distribution characteristics of the electric field of; the ladder-TM_{11} (a), ladder-TM_{51} (b), and circle-TM_{03} (c).

In the development of THz VEDs, it is critical to prepare a large-scale beam tunnel. This reduces thermal damage caused by channel interception and alleviates the requirement for a high current density electron beam generated by the electron optical system. As can be clearly seen from Fig. 3(a) and (b), by trying to project a larger-sized beam tunnel, the HF field strength decays rapidly across the beam tunnel and the E_z - field is difficult to evenly concentrate near the central axis. The above two disadvantageous phenomena can be avoided in the novel disk-load coupled cavity structure, due to its axial symmetry and more concentrated electric field distribution characteristics, as shown in Fig. 3(c). Moreover, since the radial field distribution in the cross section is a Bessel function, the axial electric field of a circular cavity is strongest in and near the center axis of the cavity in the case of higher modes. As a result, it is not only easier to suppress the competition of the fundamental mode, but also reduces the ohmic losses caused by the surface current on the cavity wall while having a larger power capacity.

The inherent quality factor Q_0 and the beam-mode coupling K of the resonant circuit are important indexes that capture the energy transfer efficiency between the HF field and electron beam [28]. In slow-wave resonant devices, the energy storage and loss of the cavity are reflected by the Q_0. The beam-mode coupling K is determined by the circuit characteristic impedance, expressed as

$$K = \frac{R}{Q} = \frac{(\int E_z \cdot dl)^2}{2\omega W} \quad (1)$$

which is a measure of the E_z field acting on the electrons for a given total stored energy W and angular frequency ω [23], [29]. Fig. 4 shows the Q_0, K, and $Q_0 \times K$ of the three circuits after CST post-processing calculations [23]. For the ladder-TM_{11} circuit, a high field energy density in a small cavity size results in higher K, but it also increases the risk of vacuum breakdown, which is very unfavorable to the stable work of the device. Additionally, the low Q_0 poses severe challenges related to increasing output power and electronic efficiency. Corresponding the ladder-TM_{51} circuits, although a high Q_0 is obtained from increasing the cavity volume, the axial HF field energy in the interaction area is lower due to the trigonometric function field distribution in the radial direction of the cross-section, which will result in a lower K and thus make it possible to be suppressed by fundamental modes. The circular quasi-TM_{03} circuit of the disk-loaded coupling cavity has both favorable cavity energy storage and beam-mode coupling. This ensures that it has a higher beam-wave interaction capability and operational stability compared to the other two more common circuits.

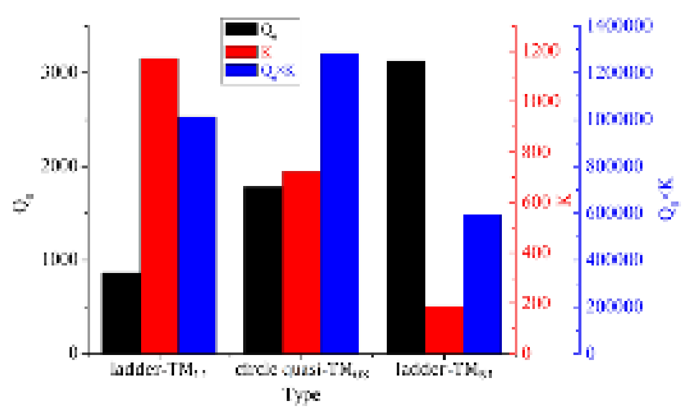

Fig. 4. The inherent quality factor Q_0, beam-mode coupling K, and interaction impedance $Q_0 \times K$ corresponding to the three types.

B. *Beam-Wave Synchronization*

The beam-wave synchronization is the key to realizing efficient beam-wave interaction and stable operation. Fig. 5 shows the dispersion characteristics of the THz extended interaction circuit. The curve is displayed as three dash lines with square, dot and triangular markers associated with the quasi-TM_{01}, quasi-TM_{02} and quasi-TM_{03} modes, respectively. Only the marks represent the modes, not the dashed segments between the marks. The axial mode was chosen as the 2π mode as it provided equal direction to the electric field at each gap for enhanced modulation of the electron beam.

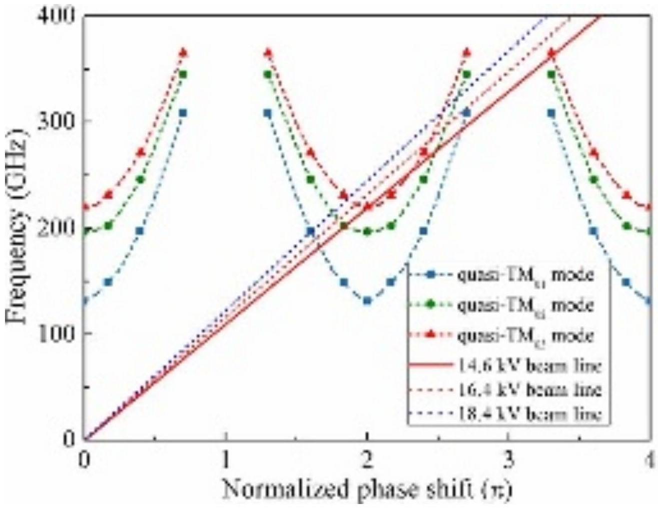

Fig. 5. Dispersion diagram of the interaction circuit.

When the electron beam passes through the gap of the resonant cavity, it will not only be affected by the HF electric field and undergo velocity modulation, but also be accompanied by density modulation. When passing through the gap, the electrons that are accelerated will consume HF field energy, and only those electrons that are decelerated will convert part of their energy into HF energy. The energy exchange between the electron beam and the HF electric field is expressed in terms of the beam-loading conductance G_e. Negative G_e indicates that the electrons have converted their DC energy to HF field energy, which implies that there will be net energy flowing to the circuit [23]. It can be obtained from

$$G_e = \frac{1}{8}\frac{\beta_e}{\beta_q} G_0\left[\left|M_-^2(\beta_e - \beta_q)\right| - \left|M_+^2(\beta_e + \beta_q)\right|\right] \quad (2)$$

where $G_0 = I_0/U_0$ (I_0 is the DC electron beam current and U_0 is the DC electron beam voltage). $\beta_e = \omega/v_e$ and $\beta_q = \omega_q/v_e$ are the propagation constants of the DC electron beam and reduced plasma respectively. G_e is completely determined by the coupling coefficient M and its variation with the DC electron beam voltage. $M_-(\beta_e - \beta_q)$ and $M_+(\beta_e + \beta_q)$ are the coupling coefficients of fast and slow space charge waves respectively [23], [29], expressed as

$$M_\pm(\beta_e \pm \beta_q) = \frac{\int_{-\infty}^{+\infty} E_z(\xi) e^{j(\beta_e \pm \beta_q)\xi} d\xi}{\int_{-\infty}^{+\infty} |E_z(\xi)| d\xi} \quad (3)$$

Where the $E_z(\xi)$ is the axial electric field at the cavity gap. Generally, g_e is introduced to express the ability of energy transfer from the beam to the circuit. It is the ratio of beam-loading conductance G_e to DC beam conductance G_0. Fig. 6 shows the variation of the g_e with a beam voltage of the quasi-TM_{01}, quasi-TM_{02} and quasi-TM_{03} modes. When the peak value of g_e is negative, it indicates that the interaction circuit is most likely to obtain energy from the electron beam, which will be the premise for the start of oscillation. It can be seen from the Fig. 6 that the negative value regions of the g_e of the three modes do not overlap with each other. This implies that the circuit will not be interfered by low-order modes when working in quasi-TM_{03} mode. Furthermore, the negative peak value of g_e of the quasi-TM_{03} mode is even larger than the other two modes, which indirectly proves its higher circuit characteristic impedance. The optimal working voltage of the quasi-TM_{03} mode interaction circuit is around 16 kV, which is also in line with the working range shown in the dispersion diagram.

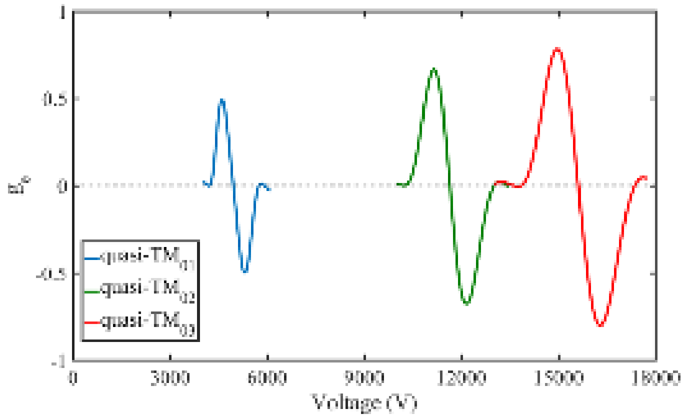

Fig. 6. Normalized g_e as a function of electron beam voltage U_0 with the quasi-TM_{01}, quasi-TM_{02} and quasi-TM_{03} modes.

C. *PIC Simulation*

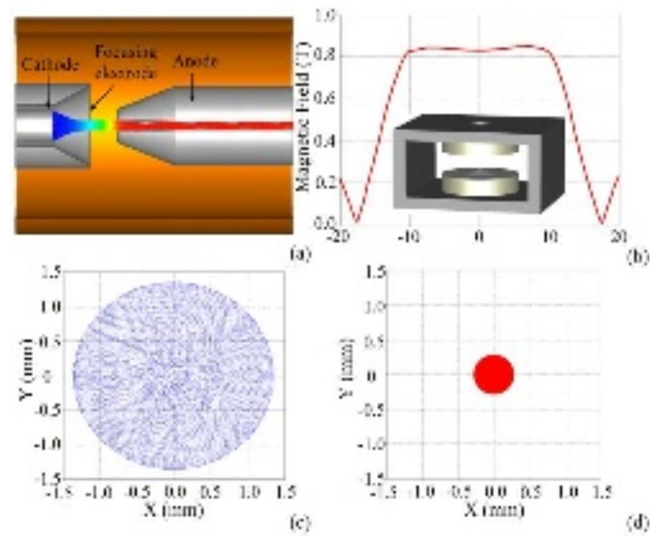

Fig. 7. The formation and transmission of the electron beam. (a) Electronic optical system. (b) Magnetic field intensity distribution of the permanent magnetic field on the axis. Inset: simulation model of the permanent magnet. (c) The size of the electron beam spot on the cathode surface. (d) Electron beam spot size in the anode plane.

The formation and transmission of the electron beam is a key point for the further experiment consideration. As shown in Fig.

7, the electron beam is first compressed by the focusing electrode and then accelerated by the anode before entering the beam tunnel. Here, the electron beam is further compressed by the focusing magnetic field, which is then converged to the size required by the device. The electron beam cross-section is compressed from the cathode emission area of 1.69π mm^2 into a beam spot of approximately 0.09π mm^2, as shown in Fig. 7(c) and (d). Fig. 7(b) shows the permanent magnet designed for the focusing and transmission of the electron beam. The magnetic material was NdFeB [16]. The maximum magnetic on-axis field strength was 0.85 T.

The performance of the THz device has been analyzed using the PIC solver. As shown in Fig. 7(a), an electron beam with a current of 0.65 A (initial current density of ~12.2 A/cm^2) is focused and injected into the interaction circuit at a voltage of 16.4 kV which is slightly higher than the calculated beam voltage from the dispersion curve. The oxygen-free copper is used as the metal background material for the device with a conductivity of 5.96 $\times 10^7$ S/m. When the synchronous condition of the circuit was satisfied, the kinetic energy of the electronic current will be converted to the quasi-TM_{03} mode HF field energy. Fig. 8 shows the power conversion of the HF field and particle in the slow-wave cavity. With the stable beam interaction between the electron beam and the electromagnetic wave of the specific frequency, the output waveguide will generate continuous electromagnetic radiation in TM_{01} mode. As shown in Fig. 9, an output power over 2.45 kW is obtained at 219.12 GHz, and the output signal spectrum shows mode purity, with a notable absence of any spurious and unwanted additional modes. The beam-wave interaction efficiency is about 23%.

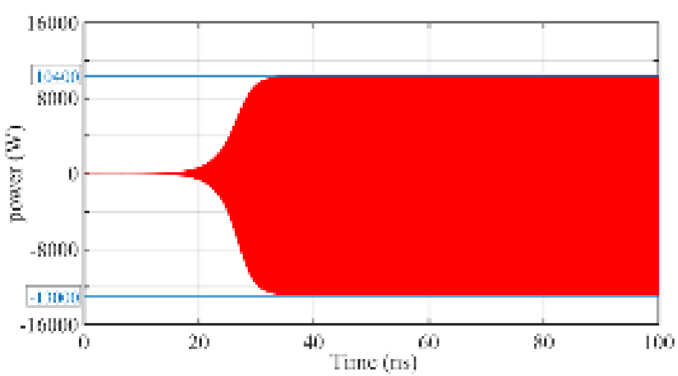

Fig. 8. Wave-particle power transfer.

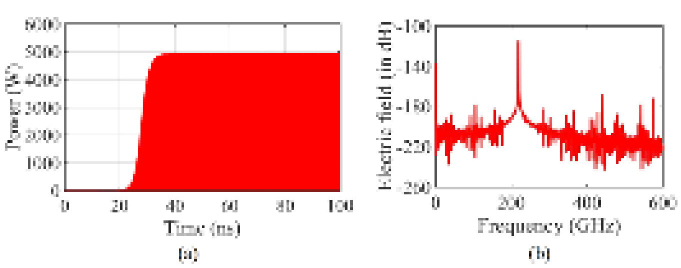

Fig. 9. (a) Signal of power amplitude at the output window. (b) Output signal spectrum.

In practice, the surface loss in metals varies with the surface roughness. In the numerical simulation of THz devices, empirical and reduced effective conductivity values are usually used to replace the additional ohmic loss due to surface roughness. Joye *et al.* have found that the assumption of a 50% reduction in conductivity is consistent with cold-test measurements at 220 GHz [25]. Further considering the ohmic loss and power drop caused by the surface roughness, we use the background material with a conductivity of 2.98 $\times 10^7$ S/m in the rough surface. PIC simulation results show that the circuit can generate over 1.23kW output power at 219.13GHz in the case of low effective conductivity. Compared to the lossy oxygen-free copper material with nearly smooth surface used at lower frequencies, the output power and the beam-wave interaction efficiency would be attenuated by about 50% when the HF surface roughness is considered. The reduction in effective conductivity caused by the surface roughness will also cause the change of operating frequency. However, the change of the operating frequency in the THz range is not obvious for the two different conductivity conditions.

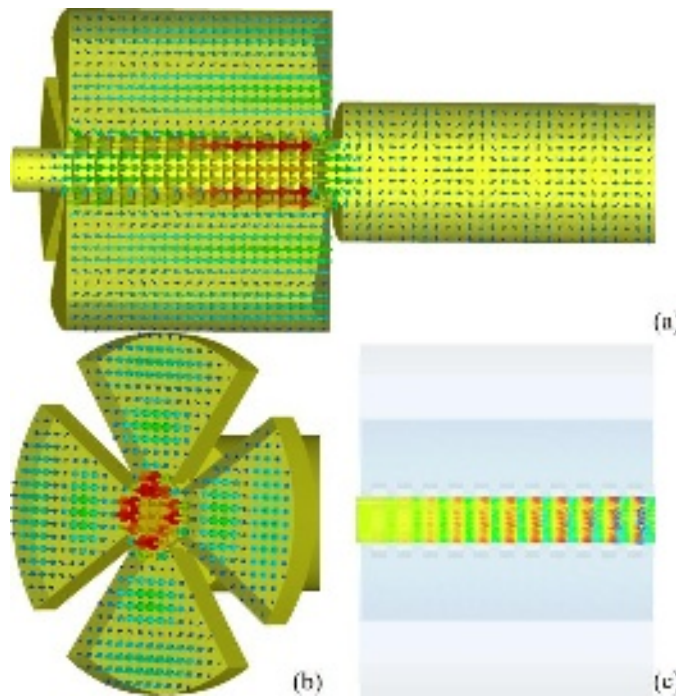

Fig. 10. Electric field arrows distribution at (a) longitudinal section and (b) transverse section, and (c) beam trajectory in the cavity of the device after stable oscillation.

Fig. 10 shows that electron bunching occurs in the cavity when the electron beam interacts with the electromagnetic wave of the specific frequency. The energy coupling of electromagnetic wave is realized by the theory of aperture diffraction. As shown in Fig 10(a) and (b), the maximum axial field energy of the quasi-TM_{03} mode is coupled to the output waveguide, and electromagnetic radiation is finally generated in the form of TM_{01} mode. Here, a large number of modes can be excited in the output cylindrical waveguide by aperture diffraction coupling. However, when analyzing the possible modes whose cut-off frequency is lower than the operating frequency, we found that all modes can be ignored except the TM_{01} mode, because their output power is very weak and almost zero. The 'probe' function could be used to monitor the field information in the cavity. Fig. 11 shows the electric field frequency spectrum and the electric field amplitude at the cavity gap. Our simulations show, the maximum field strength of the cavity is 1.08 $\times 10^7$ V/m, which is less than the vacuum breakdown field strength. Combining the dispersion diagram, output signal spectrum, electric field distribution and beam trajectory after stable oscillation, simulation results show that this novel THz extended interaction device for the disk-loaded coupled cavity can be stable with the quasi-TM_{03} mode operation.

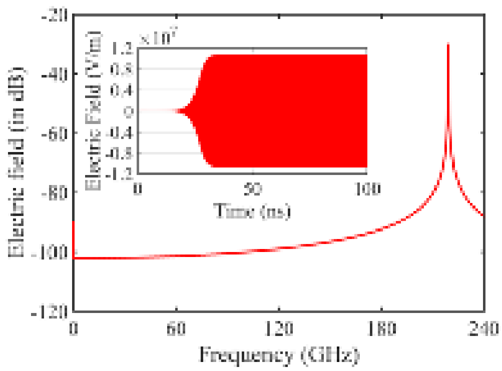

Fig. 11. The frequency spectrum at the gap where the electric field is the strongest in the cavity. Inset: the E_z - field amplitude.

III. Conclusion and Discussion

A high-efficiency THz extended interaction device capable of high power radiation output has been described. By operating in a higher-order mode, high power capacity has been obtained and the axial field energy has been concentrated on and near the central axis compared to conventional VEDs. Furthermore, the present device provides a large-scale beam tunnel that can support efficient energy conversion between the electron beam and the HF field; a significant breakthrough in the engineering of coherent electromagnetic radiation sources. Although the sheet electron beam may also provide the same level of beam tunnel capacity, it is extremely challenging to compress and focus the electrons due to its narrow and flat structure design. Compared with the previous extended interaction devices that are dominated by lateral output systems [23], the maximum axial field energy of the quasi-TM_{03} mode is coupled to the output waveguide. It not only can extract the high HF energy output but also reduces the challenges associated with device design and assembly. In the above analysis and research, based on the TM mode electric field theory of the circular waveguide resonator, the quasi-TM_{03} mode interaction circuit is designed. Although we do not rule out the possibility of higher-order modes such as TM_{04} and TM_{05} to obtain higher power and efficiency, the risk of vacuum breakdown and the challenge of suppressing mode competition will be significantly increased. Therefore, as a THz radiation source device with both high electronic efficiency and powerful radiation output, the TM_{03} mode is the best choice. Higher-order modes such as TM_{04} and TM_{05} are more likely to be used in low output power devices that require low current. Here, a kilowatt-level, 0.22 THz radiation source with a 11.5% electron efficiency has been verified by PIC simulations. Further detailed consideration of adding mode converter to achieve the beam-wave separation [30], improving the multistage depressed collector to enhance the electronic efficiency, will likely manifest in functional enhancements and improved applicability.

To sum up, the disk-loaded coupled cavity circuit operating in quasi-TM_{03} mode shows worthwhile potential in overcoming the frequency limitations, improving the efficiency of beam-wave interaction and operating stability. It is expected to be used to develop coherent electromagnetic radiation sources with higher frequency, higher power and higher efficiency.

ACKNOWLEDGMENTS

This work was supported in part by the National Key Research and Development Program of China under Grant 2019YFA0210202, in part by National Natural Science Foundation of China under Grant 61771096, in part by Sichuan Science and Technology Program under Grant 2021YJ0096, and in part by the Fundamental Research Funds for the Central Universities under Grant ZYGX2019J012 and Grant ZYGX2019Z006.

DATA AVAILABILITY

The data that support the findings of this study are available from the corresponding author upon reasonable request.

References

[1] P. H. Siegel, “Terahertz technology,” *IEEE Trans. Microw. Theory Techn.*, vol. 50, no. 3, pp. 910-928, Mar. 2002. doi: 10.1109/22.989974.

[2] J. H. Booske, “Plasma physics and related challenges of millimeter-wave-to-terahertz and high power microwave generation,” *Phys. Plasmas*, vol. 15, no. 055502, pp. 1-16, May. 2008. doi: 10.1063/1.2838240.

[3] L. Krier, I. G. Pagonakis, K. A. Avramidis, G. Gantenbein, S. Illy, J. Jelonnek, J. Jin, H. P. Laqua, A. Marek, D. Moseev, and M. Thumm, “Theoretical investigation on possible operation of a 140 GHz 1 MW gyrotron at 175 GHz for CTS plasma diagnostics at W7-X,” *Phys. Plasmas*, vol. 27, no. 11, p. 113107, Nov. 2020. doi: 10.1063/5.0022151.

[4] J. H. Booske, R. J. Dobbs, C. D. Joye, C. L. Kory, G. R. Neil, G. S. Park, J. Park, and R. J. Temkin, “Vacuum electronic high power terahertz sources,” *IEEE Trans. Terahertz Sci. Technol.*, vol. 1, no. 1, pp. 54-75, Sep. 2011. doi: 10.1109/TTHZ.2011.2151610.

[5] P. H. Siegel, “Terahertz technology in biology and medicine,” *IEEE Trans. Microw. Theory Techn.*, vol. 52, no. 10, pp. 2438-2447, Oct. 2004. doi: 10.1109/TMTT.2004.835916.

[6] H.-J. Song and T. Nagatsuma, “Present and future of terahertz communications,” *IEEE Trans. Terahertz Sci. Technol.*, vol. 1, nol. 1, pp. 256-263, Sep. 2011. doi: 10.1109/TTHZ.2011.2159552.

[7] K. B. Cooper, R. J. Dengler, N. Llombart, B. Thomas, G. Chattopadhyay, and P. H. Siegel, “THz imaging radar for standoff personnel screening,” *IEEE Trans. Terahertz Sci. Technol.*, vol. 1, no. 1, pp. 169-182, Sep. 2011. doi: 10.1109/TTHZ.2011.2159556.

[8] M. Tonouchi, “Cutting-edge terahertz technology,” *Nature Photon*, vol. 1, nol. 2, pp. 97-105, Feb. 2007. doi: 10.1038/nphoton.2007.3.

[9] R. K. Parker, R. H. Abrams, B. G. Danly, and B. Levush, “Vacuum electronics,” *IEEE Trans. Microw. Theory Techn.*, vol. 50, no. 3, pp. 835-845, Mar. 2002. doi: 10.1109/22.989967.

[10] G. X. Shu, H. Yin, L. Zhang, J. P. Zhao, G. Liu, A. D. R. Phelps, A. W. Cross, and W. He, “Demonstration of a planar W-band, kW-level extended interaction oscillator based on a pseudospark-sourced sheet electron beam,” *IEEE Electron Device Lett.*, vol. 39, no. 3, pp. 432-435, Mar. 2018. doi: 10.1109/LED.2018.2794469.

[11] X. Yuan, W. Zhu, Y. Zhang, N. Xu, Y. Yan, J. Wu, Y. Shen, J. Chen, J. She, and S. Deng, “A fully-sealed carbon-nanotube cold-cathode terahertz gyrotron,” *Sci. Rep.*, vol. 6, p. 32936, Sep. 2016. doi: 10.1038/srep32936.

[12] I. G. Pagonakis, K. A. Avramidis, G. Gantenbein, S. Illy, Z. C. Ioannidis, J. Jin, P. Kalaria, B. Piosczyk, S. Ruess, T. Ruess, T. Rzesnicki, M. Thumm, and J. Jelonnek, "Triode magnetron injection gun for the KIT 2 MW 170 GHz coaxial cavity gyrotron," *Phys. Plasmas*, vol. 27, no. 2, p. 023105, Feb. 2020. doi: 10.1063/1.5132615.

[13] P. Hu, W. Lei, Y. Jiang, Y. Huang, R. Song, H. Chen, and Y. Dong, "Demonstration of a watt-level traveling wave tube amplifier operating above 0.3 THz," *IEEE Electron Device Lett.*, vol. 40, no. 6, pp. 973-976, Jun. 2019. doi: 10.1109/LED.2019.2912579.

[14] D. Berry, H. Deng, R. Dobbs, P. Horoyski, M. Hyttinen, A. Kingsmill, R. MacHattie, A. Roitman, E. Sokol, and B. Steer, "Practical aspects of EIK technology," *IEEE Trans. Electron Devices*, vol. 61, no. 6, pp. 1830-1835, Jun. 2014. doi: 10.1109/TED.2014.2302741.

[15] J. Zhang, T. Z. Zhang, Y. Alfadhl, X. D. Chen, L. Zhang, H. B. Yin, and A. W. Cross, "Study on Wideband THz Backward Wave Oscillator Driven by Pseudospark-Sourced Sheet Electron Beam," *IEEE Trans. Electron Devices*, vol. 67, no. 8, pp. 3395-3402, Aug. 2020. doi: 10.1109/TED.2020.3005362.

[16] X. Xu, X. Yuan, Q. Chen, M. T. Cole, Y. Zhang, J. Xie, Y. Yin, H. Li, and Y. Yan, "A low-voltage, premodulation terahertz oscillator based on a carbon nanotube cold cathode," *IEEE Trans. Electron Devices*, vol. 67, no. 3, pp. 1266-1269, Mar. 2020. doi: 10.1109/TED.2020.2968932

[17] J. Feng, Y. Tang, D. Gamzina, X. Li, B. Popovic, M. Gonzalez, L. Himes, R. Barchfeld, H. Li, P. Pan, R. Letizia, C. Paoloni, and N. C. Luhmann, "Fabrication of a 0.346-THz BWO for plasma diagnostics," *IEEE Trans. Electron Devices*, vol. 65, no. 6, pp. 2156-2163, Jun. 2018. doi: 10.1109/TED.2018.2821683.

[18] Communications & Power Industries, Georgetown, ON, Canada. (Oct. 31, 2001). *Extended Interaction Klystrons*. [Online]. Available: https://www.cpii.com/product.cfm/4/40/156.

[19] R. Basu, L. R. Billa, R. Letizia, and C. Paoloni, "Design of sub-THz traveling wave tubes for high data rate long range wireless links," *Semicond. Sci. Technol.*, vol. 33, no. 12, p. 124009, Dec. 2018. doi: 10.1088/1361-6641/aae859.

[20] C. Paoloni and M. Mineo, "Double corrugated waveguide for G-band traveling wave tubes," *IEEE Trans. Electron Devices*, vol. 61, no. 12, pp. 4259-4263, Dec. 2014. doi: 10.1109/TED.2014.2364636.

[21] A. Roitman, D. Berry, M. Hyttinen, and B. Steer, "Sub-millimeter waves from a compact, low voltage extended interaction klystron," in *Conf. Rec. IRMMW-THz 2007*, Cardiff, U.K., Sep. 2007, pp. 892-894.

[22] Y. Yin, W. He, L. Zhang, H. Yin, and A. W. Cross, "Preliminary design and optimization of a G-band extended interaction oscillator based on a pseudospark-sourced electron beam," *Phys. Plasmas*, vol. 22, no. 7, p. 073102, Jul. 2015. doi: 10.1063/1.4926512.

[23] L. Bi, L. Meng, Y. Yin, C. Xu, S. Zhu, R. Peng, F. Zeng, Z. Chang, B. Wang, H. Li, and P. Zhang, "Design and analysis of a high-order mode ladder-type RF circuit for stable operation in a W-band extended interaction oscillator," *IEEE Trans. Electron Devices*, vol. 66, no. 1, pp. 729-735, Jan. 2019. doi: 10.1109/TED.2018.2882956.

[24] D. Gamzina, L. G. Himes, R. Barchfeld, Y. Zheng, B. K. Popovic, C. Paoloni, E. Choi, and N. C. Luhmann, "Nano-CNC machining of sub-THz vacuum electron devices," *IEEE Trans. Electron Devices*, vol. 63, no. 10, pp. 4067-4073, Oct. 2016. doi: 10.1109/TED.2016.2594027.

[25] C. D. Joye, A. M. Cook, J. P. Calame, D. K. Abe, A. N. Vlasov, l. A. Chernyavskiy, K. T. Nguyen, E. L. Wright, D. E. Pershing, T. Kimura, M. Hyttinen, and B. Levush, "Demonstration of a high power, wideband 220-GHz traveling wave amplifier fabricated by UV-LIGA," *IEEE Trans. Electron Devices*, vol. 61, no. 6, pp. 1672-1678, Jun. 2014. doi: 10.1109/TED.2014.2300014.

[26] J. Xie, L. Zhang, H. Yin, W. He, K. Ronald, A. D. R. Phelps, X. Chen, J. Zhang, Y. Alfadhl, X. Yuan, L. Meng, and A. W. Cross, "Study of a 0.35 THz extended interaction oscillator driven by a pseudospark-sourced sheet electron beam," *IEEE Trans. Electron Devices*, vol. 67, no. 2, pp. 652-658, Feb. 2020. doi: 10.1109/TED.2019.2957760.

[27] Y. Zu, X. Yuan, X. Xu, M. T. Cole, Y. Zhang, H. Li, Y. Yin, B. Wang, and Y. Yan, "Design and Simulation of a Multi-Sheet Beam Terahertz Radiation Source Based on Carbon-Nanotube Cold Cathode," *Nanomaterials*, vol. 9, no. 12, p.1768, Dec. 2019. doi: 10.3390/nano9121768.

[28] S. Li, J. Wang, G. Wang, and D. Wang. "Theoretical studies on stability and feasibility of 0.34 THz EIK," *Phys. Plasmas*, vol. 24, no. 5, p. 053107, May. 2017. doi: 10.1063/1.4983621.

[29] C. Xu, B. Wang, R. Peng, L. Bi, F. Zeng, Z. Chang, S. Zhu, Y. Yin, H. Li, and L. Meng, "Start current study of a THz sheet beam extended interaction oscillator," *Phys. Plasmas*, vol. 25, no. 7, p. 073103, Jul. 2018. doi: 10.1063/1.5027445.

[30] Q. Chen, X. Yuan, T. Yang, J. Xie, X. Xu, B. Wang, H. Li, Y. Yin, M. T. Cole, L. Meng, and Y. Yan, "Development of a Ka-band circular TM01 to rectangular TE10 mode converter," *IEEE Trans. Electron Devices*, vol. 67, no. 3, pp. 1254-1258, Mar. 2020. doi: 10.1109/TED.2020.2968347.

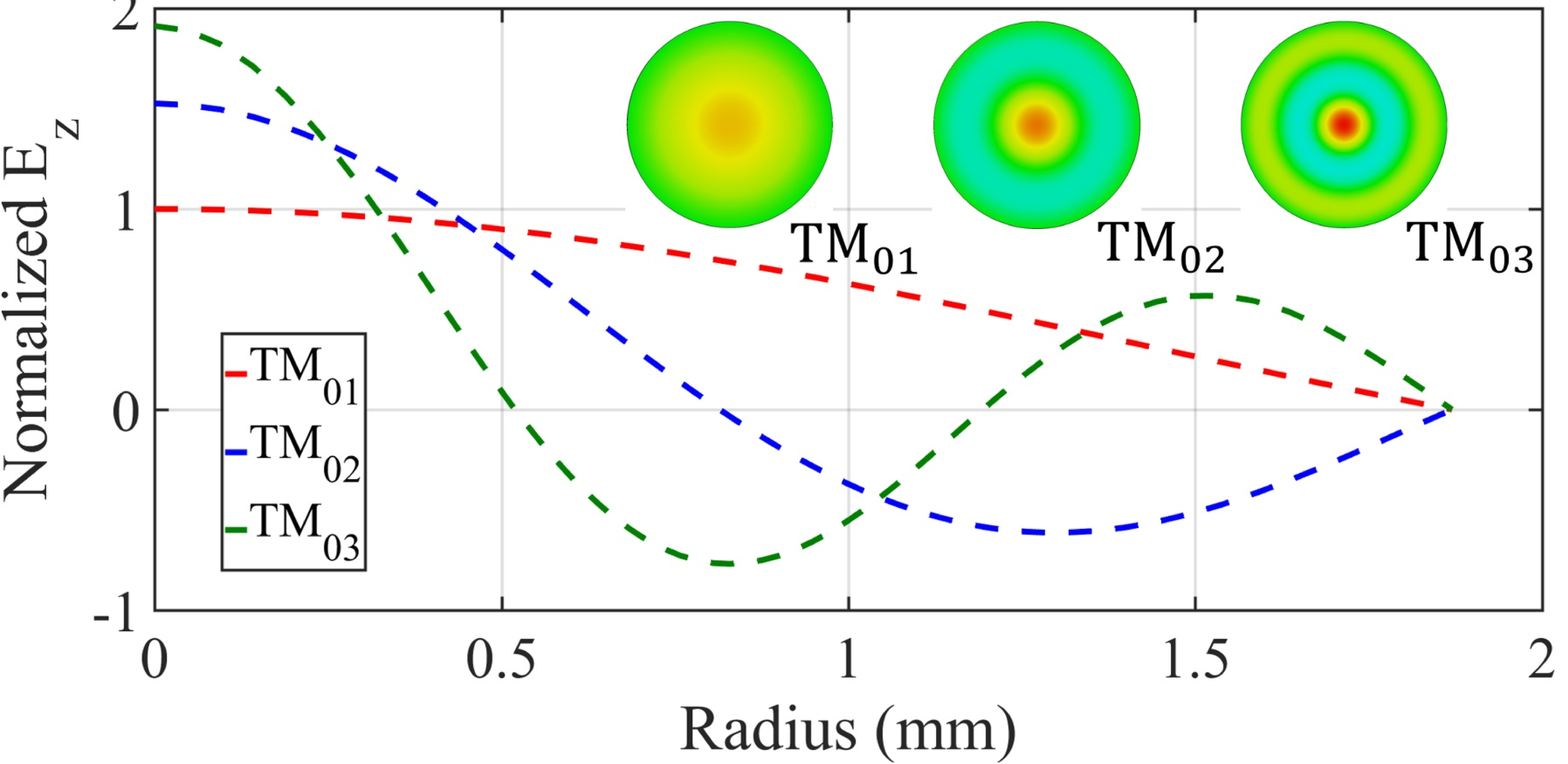

TM01
TM02
TM03
TM01
TM02
TM03
Normalized Ez
Radius (mm)
2
1
0
-1
0
0.5
1
1.5
2

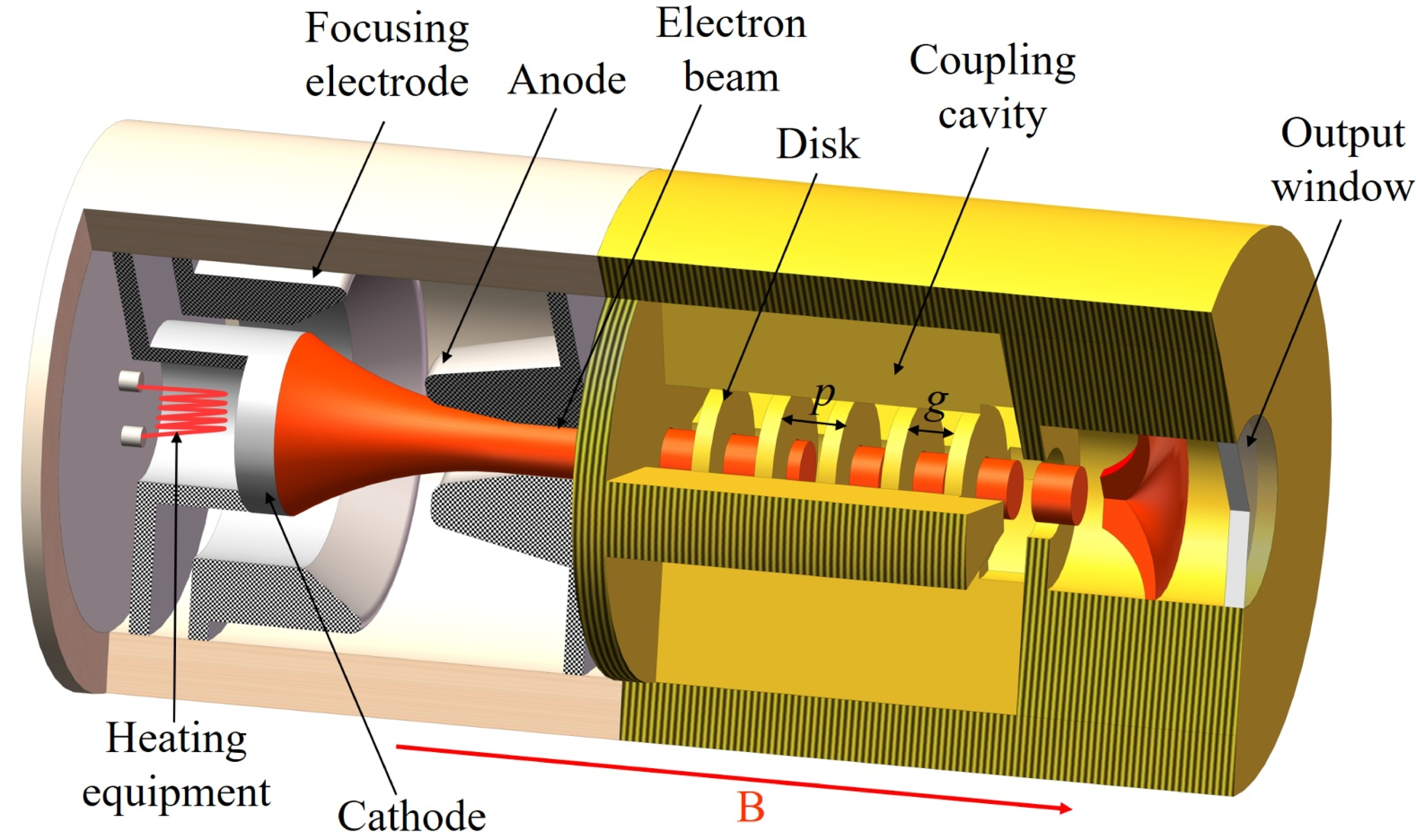

Focusing electrode
Anode
Electron beam
Coupling cavity
Disk
Output window
p
g
Heating equipment
Cathode
B

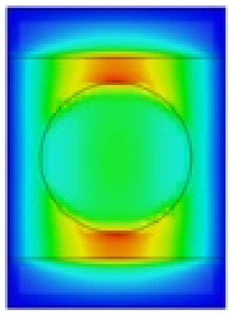

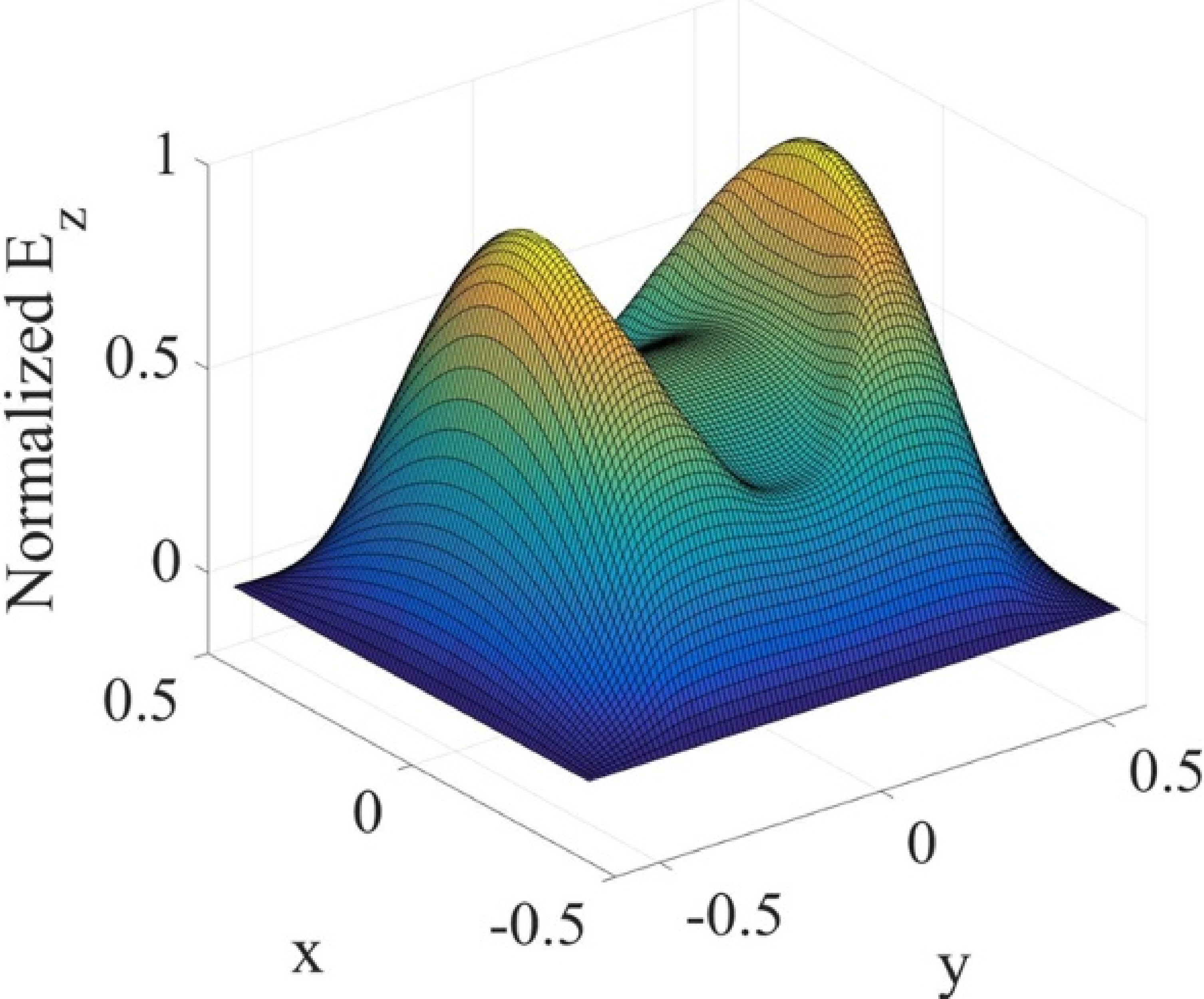

(a) $\mathbf{ladder - TM_{11}}$

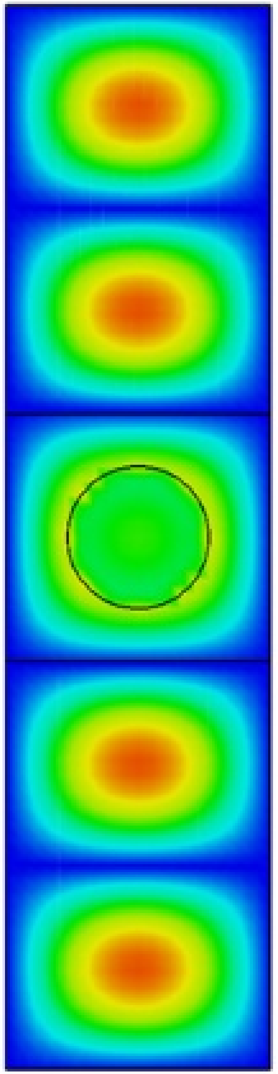

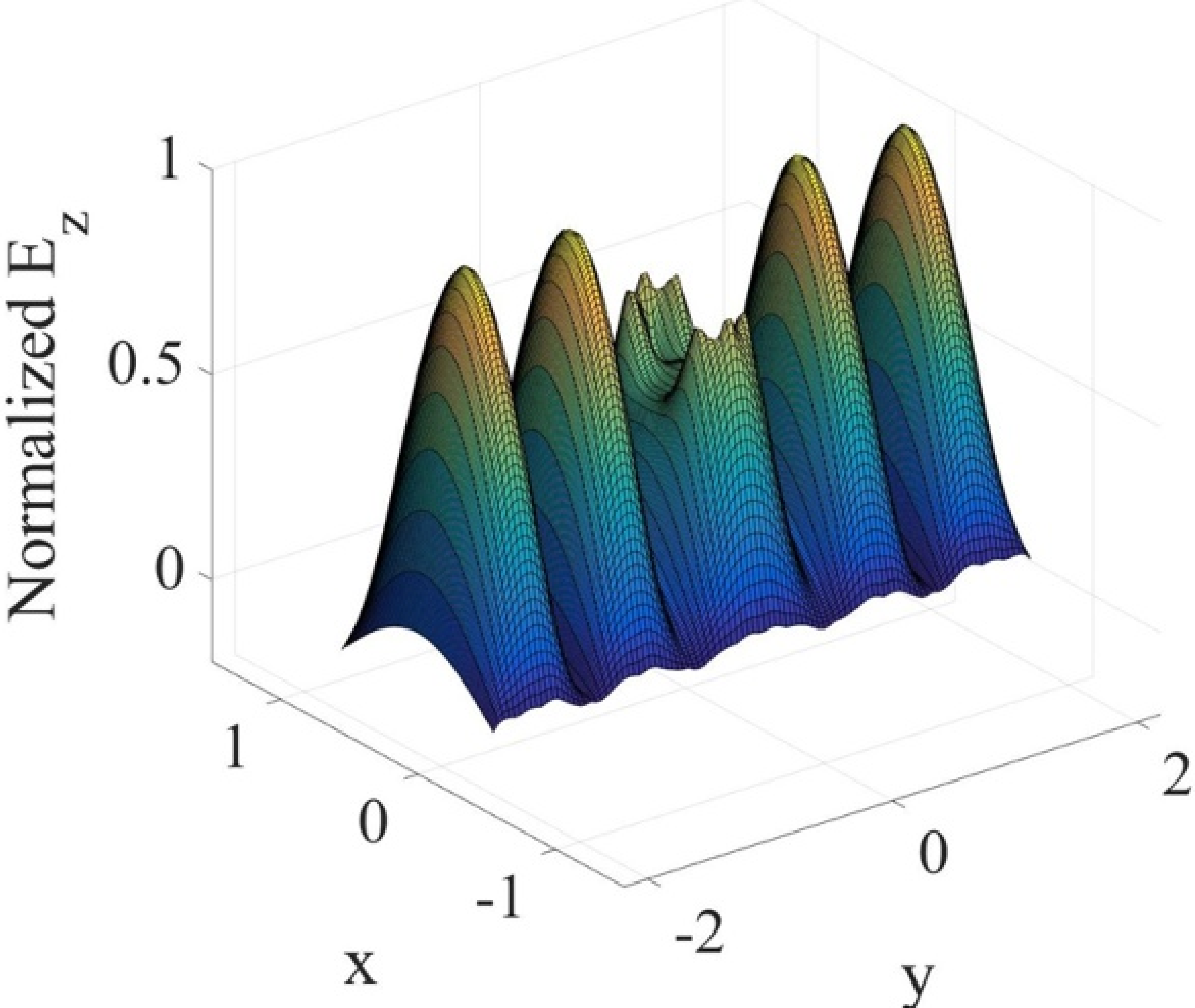

(b) $\mathbf{ladder - TM_{51}}$

(c) circle quasi − TM_{03}

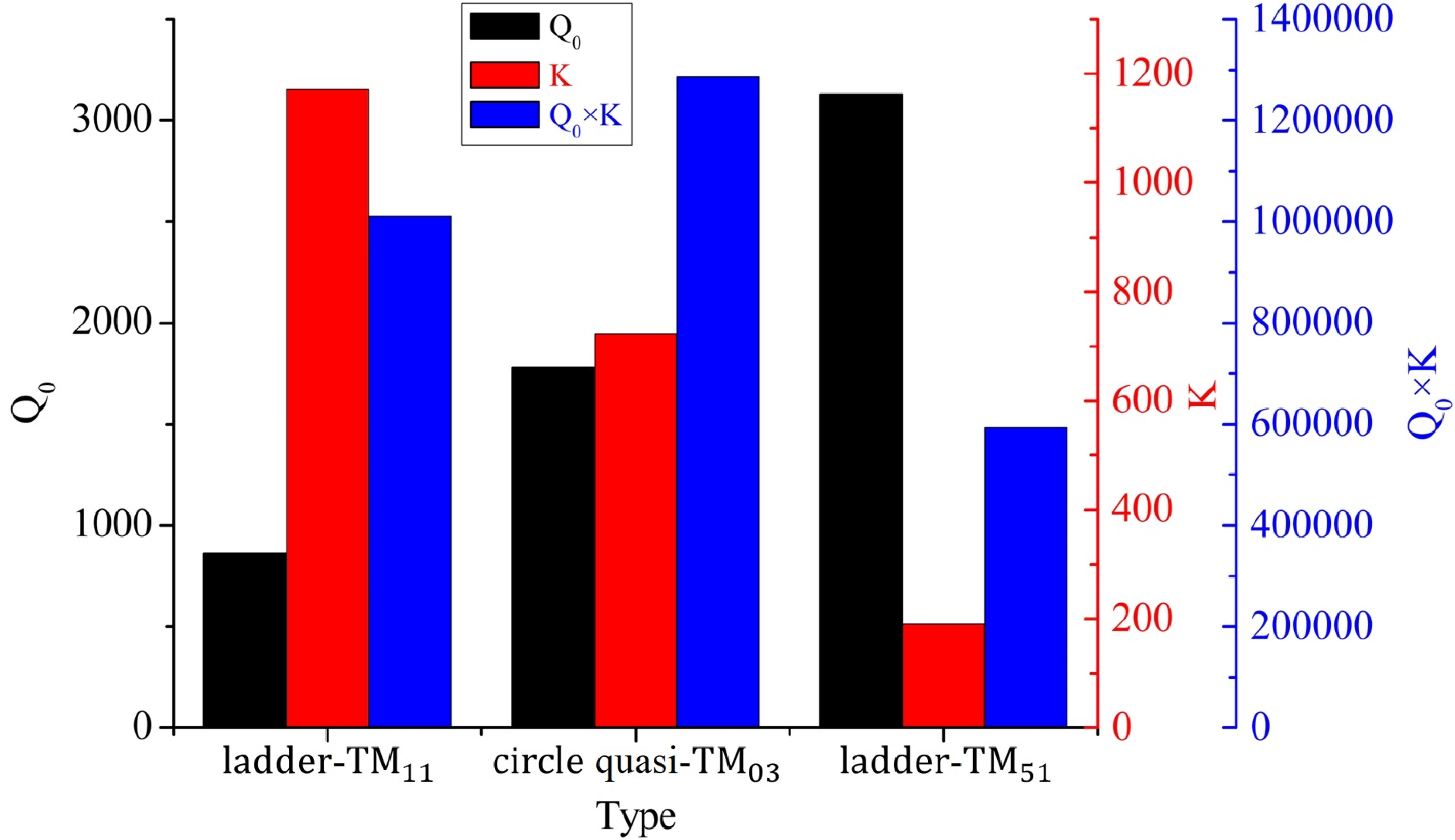

Q0
K
Q0×K
3000
2000
1000
0
1200
1000
800
600
400
200
0
1400000
1200000
1000000
800000
600000
400000
200000
0
Q0
K
Q0×K
ladder-TM11
circle quasi-TM03
ladder-TM51
Type

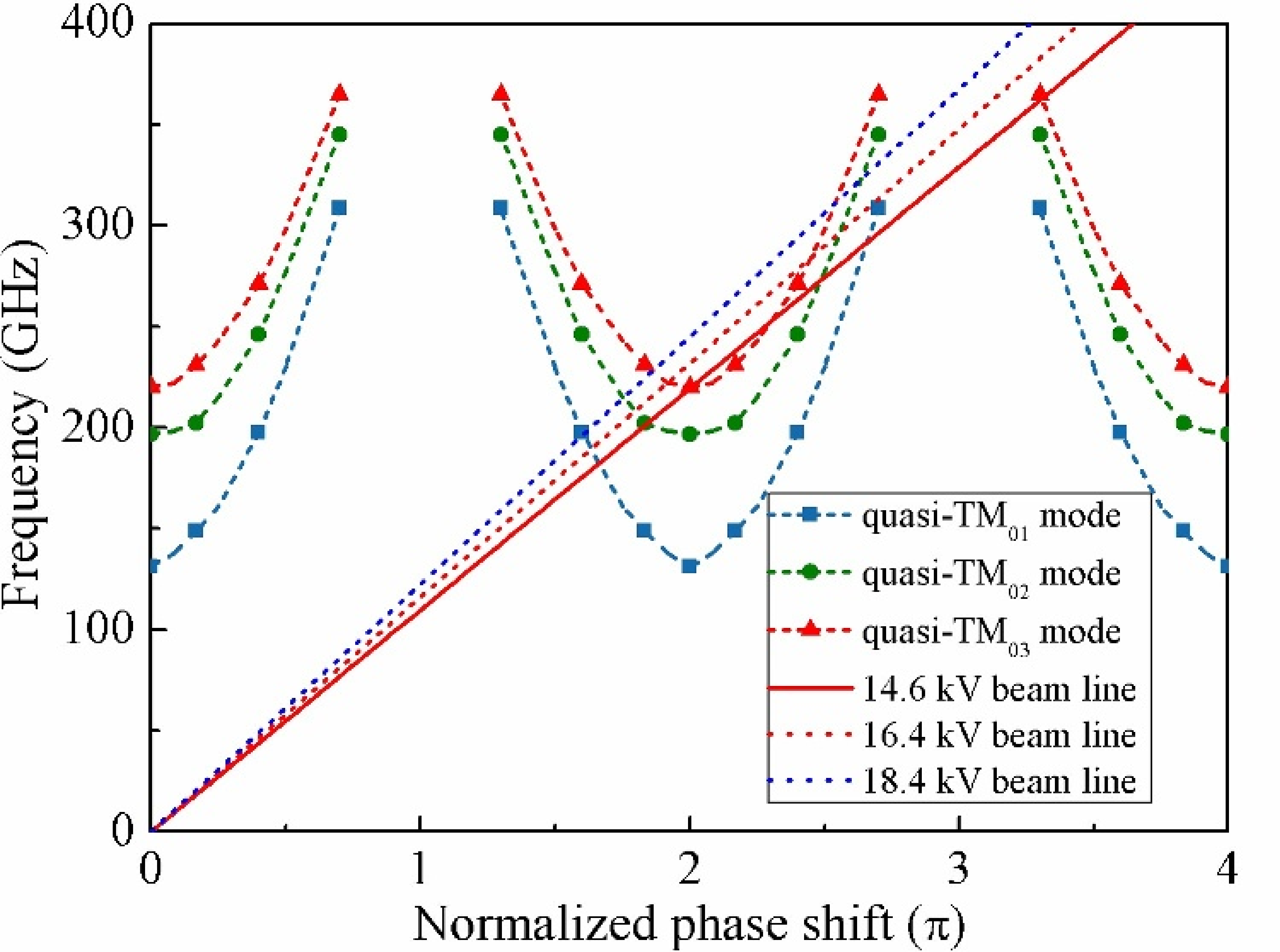

Frequency (GHz)
Normalized phase shift (π)
0
100
200
300
400
0
1
2
3
4
quasi-TM01 mode
quasi-TM02 mode
quasi-TM03 mode
14.6 kV beam line
16.4 kV beam line
18.4 kV beam line

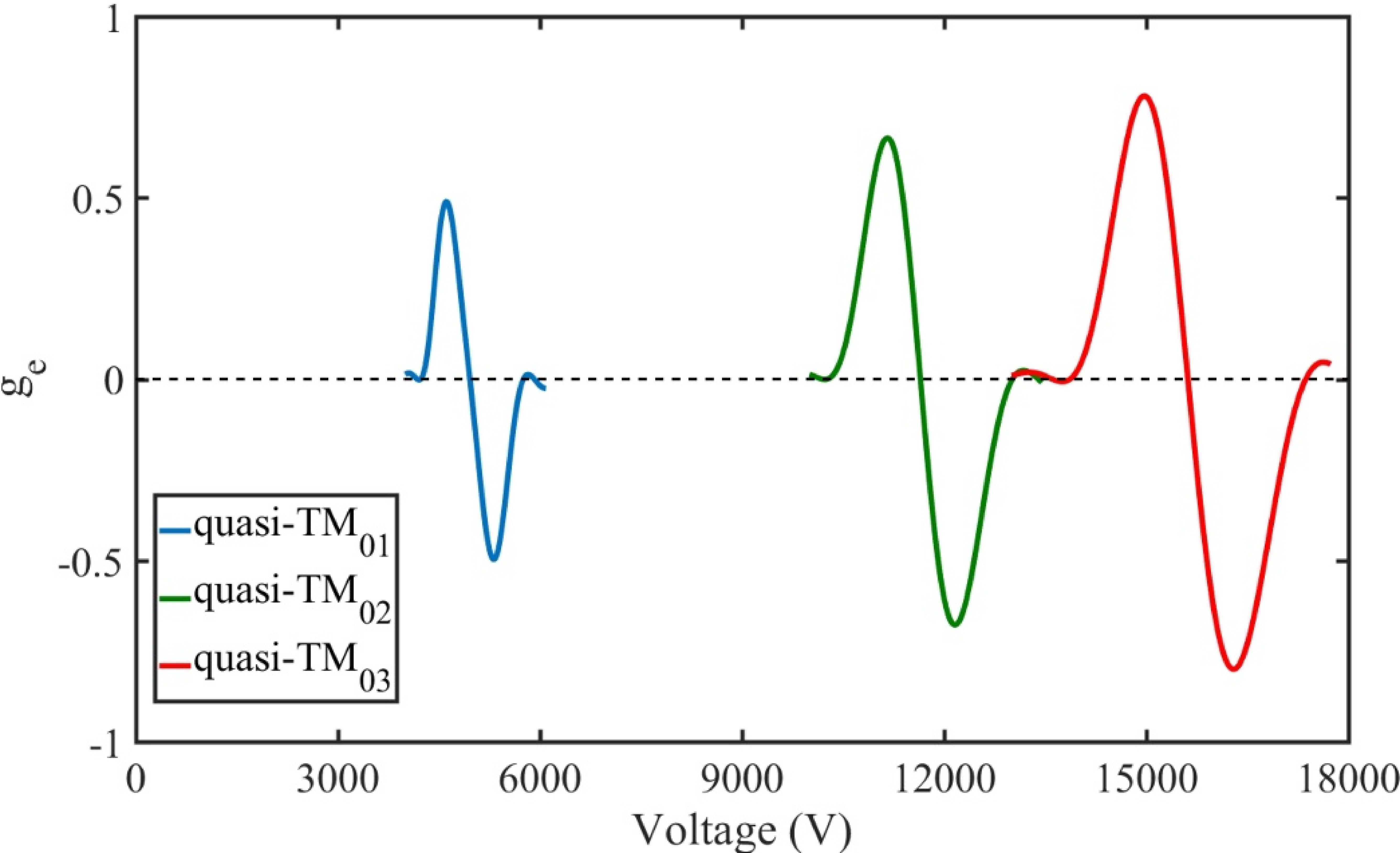

1
0.5
0
-0.5
-1
g_e
0
3000
6000
9000
12000
15000
18000
Voltage (V)
quasi-TM_{01}
quasi-TM_{02}
quasi-TM_{03}

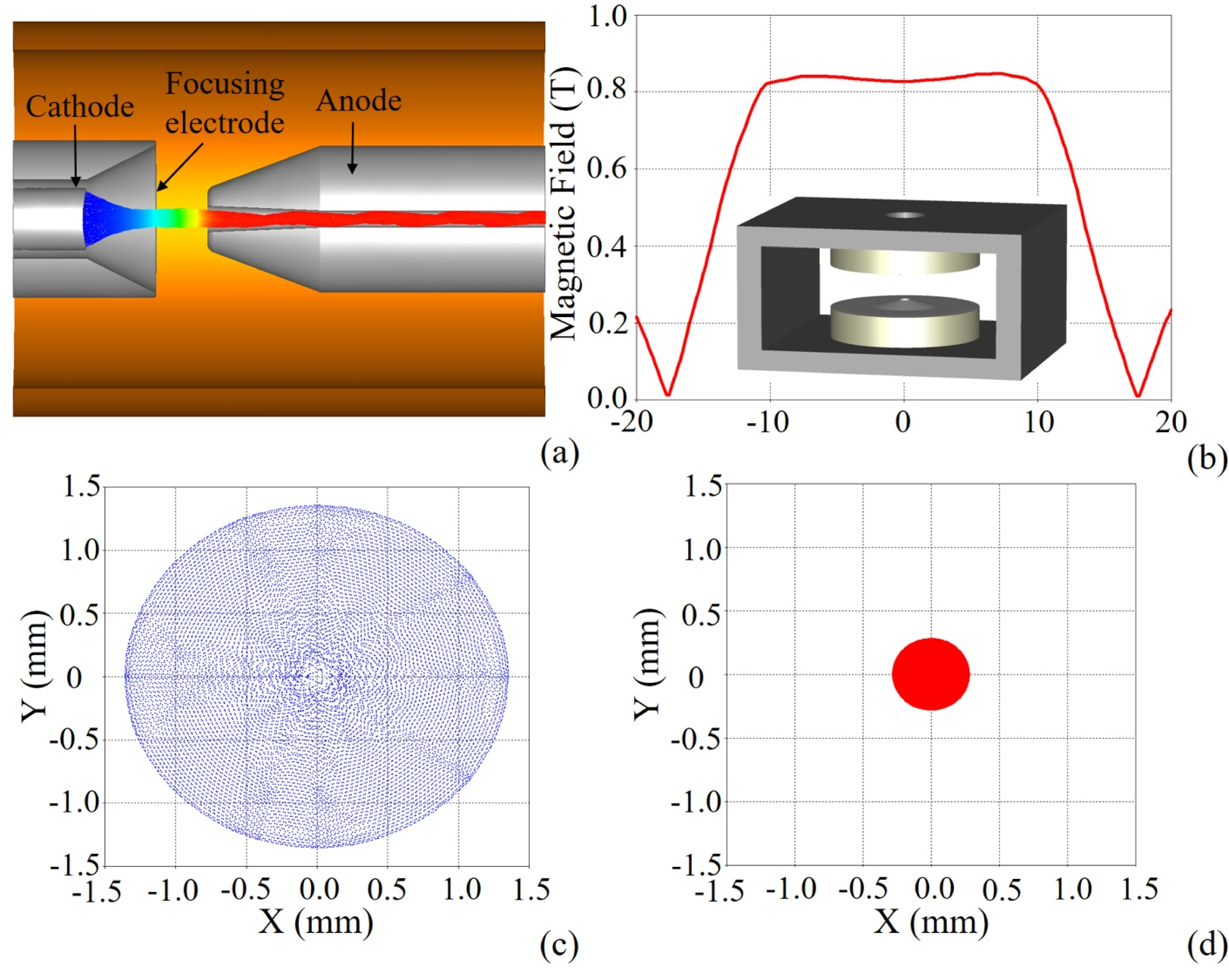

Cathode
Focusing electrode
Anode
(a)
Magnetic Field (T)
1.0
0.8
0.6
0.4
0.2
0.0
-20
-10
0
10
20
(b)
Y (mm)
X (mm)
1.5
1.0
0.5
0
-0.5
-1.0
-1.5
0.0
(c)
(d)

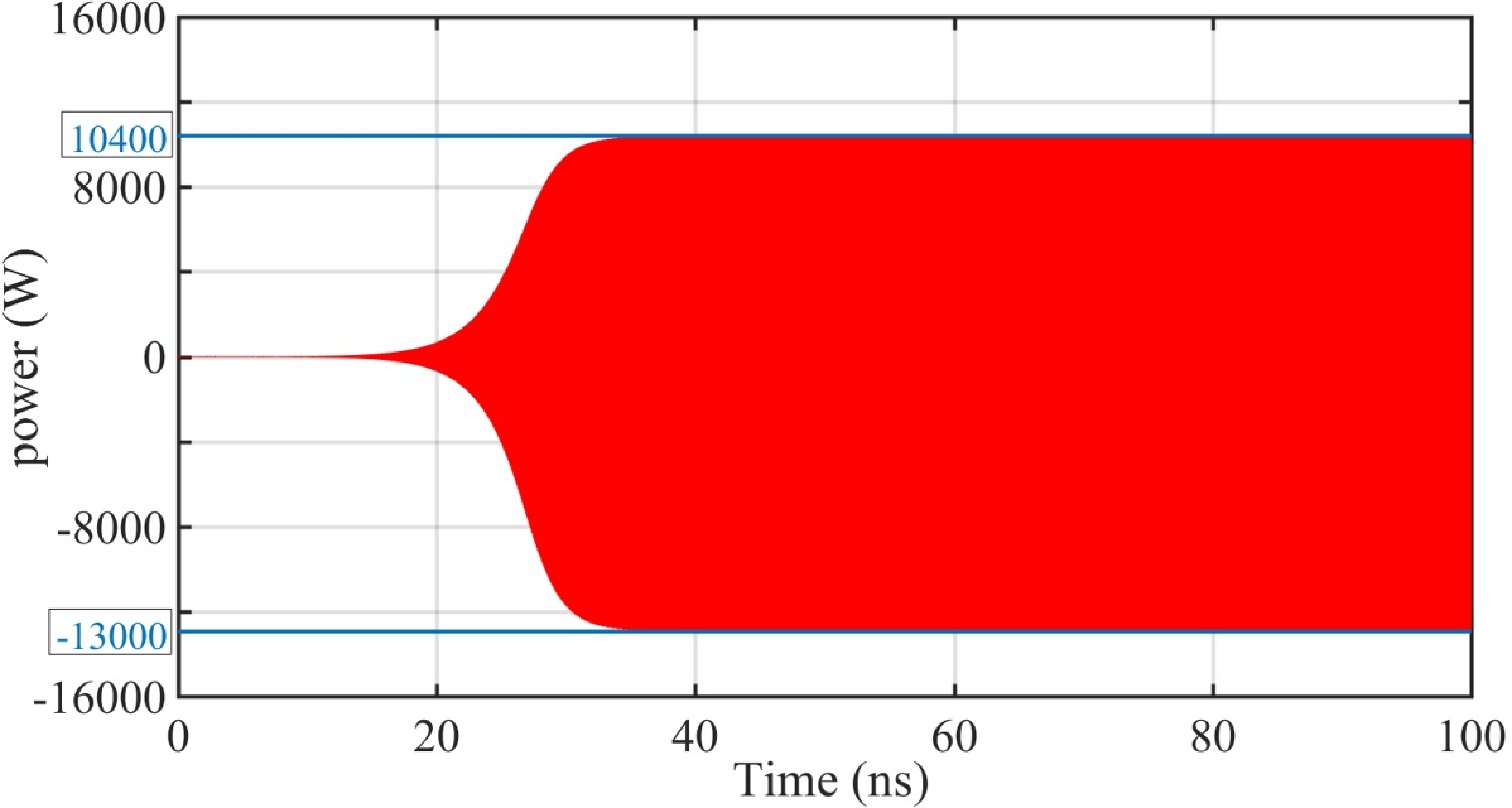
16000
10400
8000
0
-8000
-13000
-16000
power (W)
0
20
40
60
80
100
Time (ns)

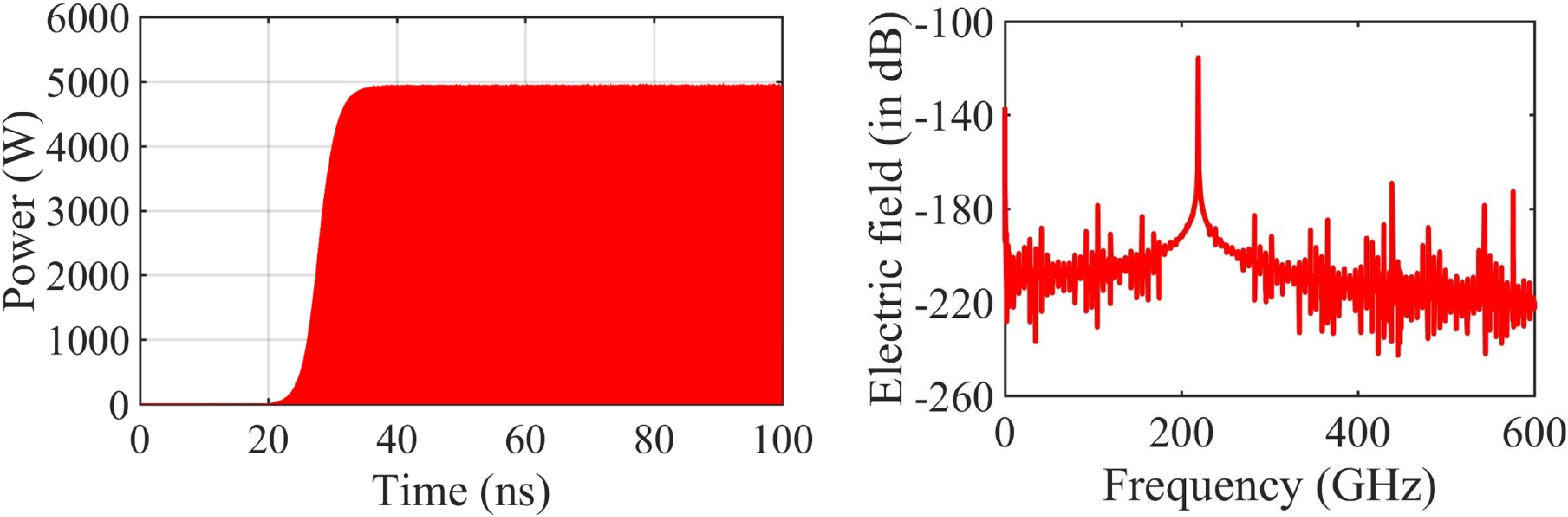

Power (W)
6000
5000
4000
3000
2000
1000
0
0
20
40
60
80
100
Time (ns)
Electric field (in dB)
-100
-140
-180
-220
-260
0
200
400
600
Frequency (GHz)

(a) (b)

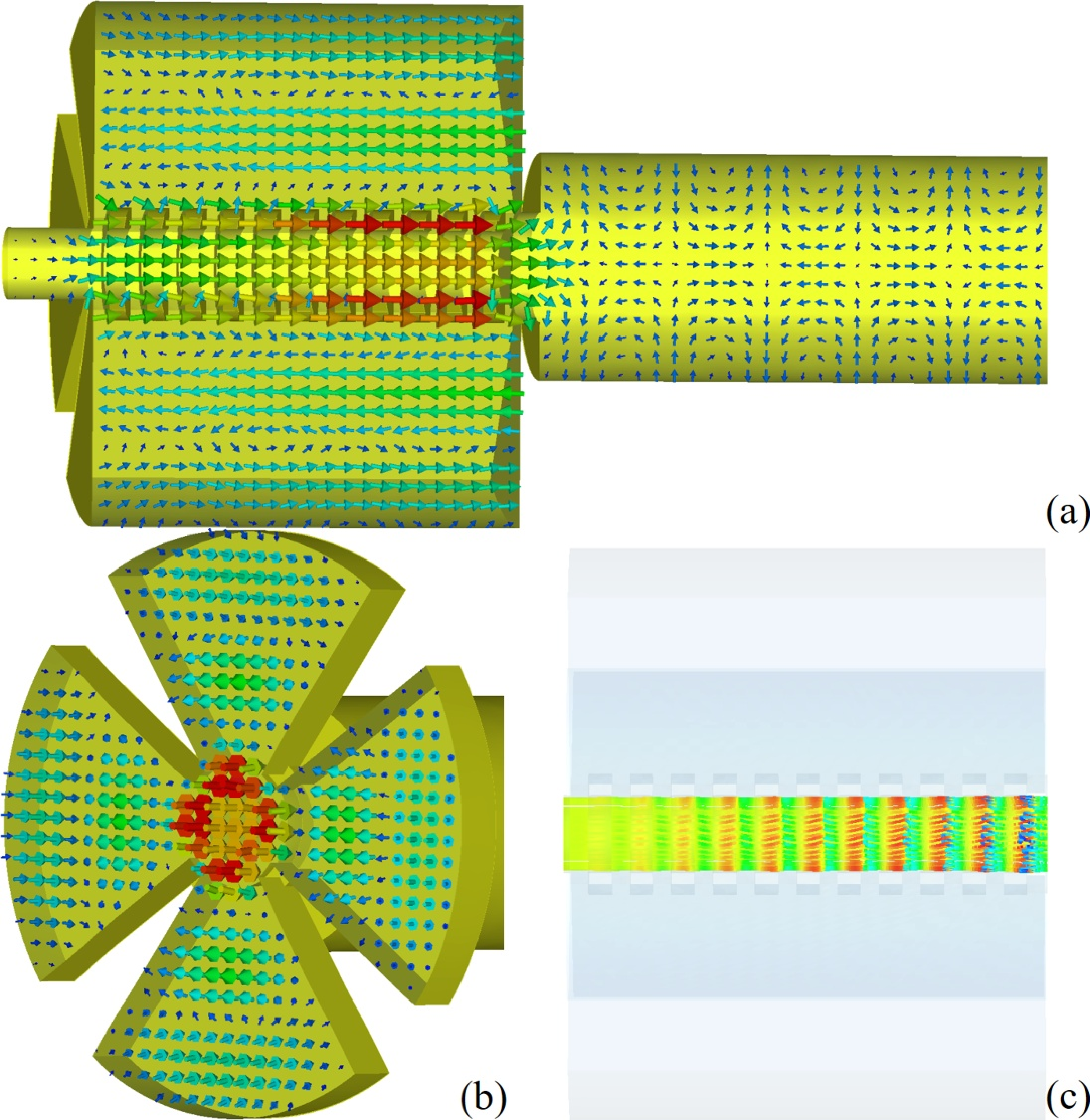
(a)
(b)
(c)

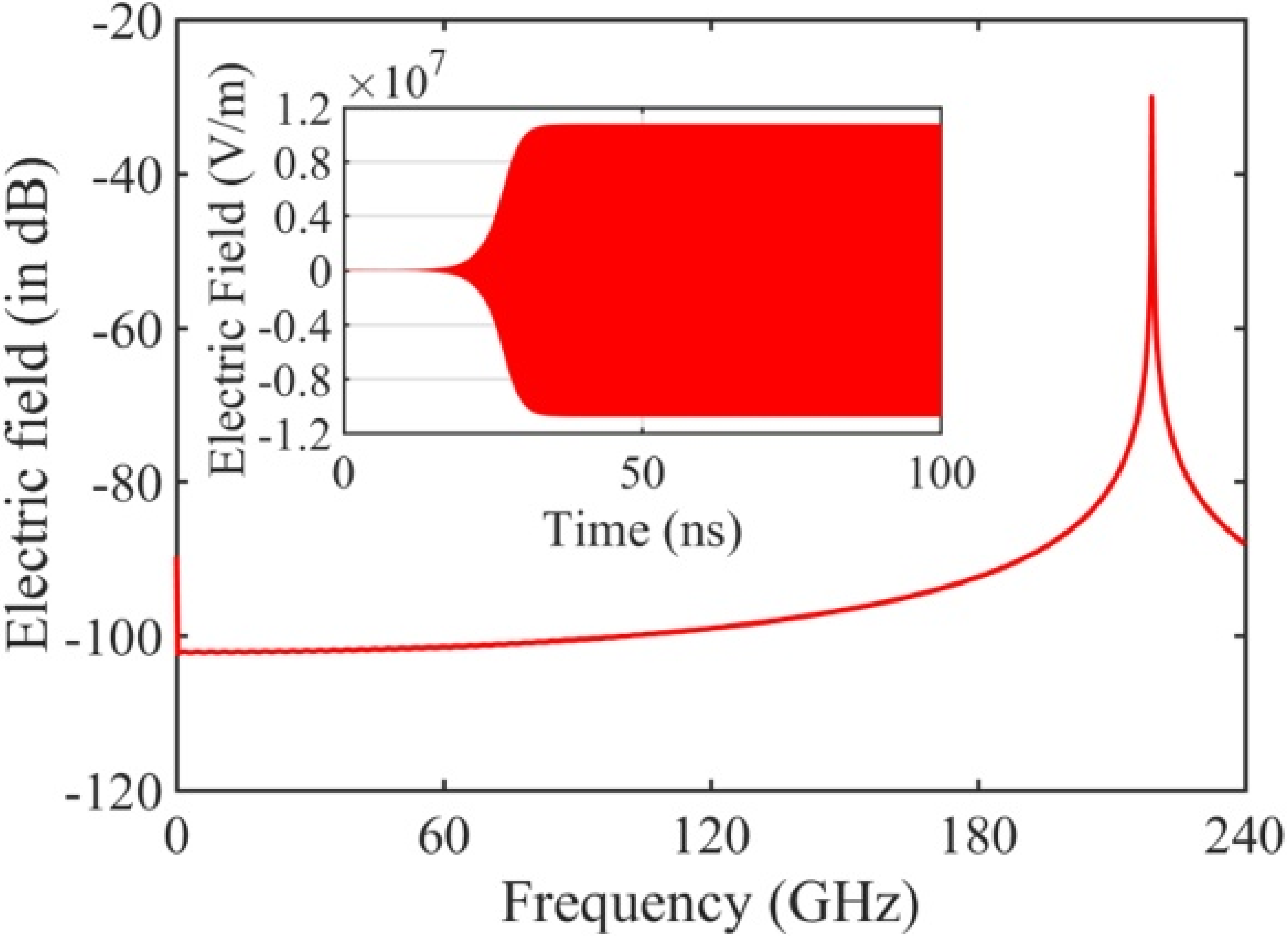

-20
-40
-60
-80
-100
-120
Electric field (in dB)
0
60
120
180
240
Frequency (GHz)
×10^7
1.2
0.8
0.4
0
-0.4
-0.8
-1.2
Electric Field (V/m)
0
50
100
Time (ns)